BJS-NF08

Modeling and Measuring Nasal Airflow

A Major Qualifying Project
submitted to Brian J. Savilonis
of the
WORCESTER POLYTECHNIC INSTITUTE
in partial fulfillment of the requirements for the
Degree of Bachelor of Science
by

Allison Hunt
Andrea Marinelli
Devin Oakes
Edward G. Roberts
Date: April 24, 2008

TABLE OF CONTENTS

AUTHORSHIP PAGE

The team would like to acknowledge each member and present each member's contribution to this report by chapter.

Chapter 1 – Andrea Marinelli

Chapter 2 – Allison Hunt, Andrea Marinelli, Devin Oakes, & Edward G. Roberts

Chapter 3 – Andrea Marinelli

Chapter 4 – Allison Hunt & Andrea Marinelli

Chapter 5 – Allison Hunt, Andrea Marinelli, Devin Oakes, & Edward G. Roberts

Chapter 6 – Andrea Marinelli, Devin Oakes, & Edward G. Roberts

Chapter 7 – Allison Hunt & Devin Oakes

Chapter 8 – Edward G. Roberts

ACKNOWLEDGEMENTS

Prof. Brian Savilonis, WPI Mechanical Engineering Department – For his continued assistance in the development and completion of this project.

Barbara Fuhrman, WPI Mechanical Engineering Department – For her assistance in obtaining supplies necessary to complete the project.

Patrick Salmon, WPI Alumnus – For his contributions to the motor program.

Tom Keller, Performance Motion Devices – For his continued assistance with motion control devices.

Dr. David Wexler, UMass Medical – For project development and support.

ABSTRACT

Approximately 20% of the world population suffers from nasal obstruction. The current method for treating this condition is an operation called a nasal turbinectomy. The effectiveness of this surgery has been evaluated mostly through patient perception and computer simulation, both of which can be inconclusive. To obtain more definitive results, pressure measurements and flow data were documented in this project using pre- and post-surgery scale models of the human nasal passages.

TABLE OF FIGURES

TABLE OF TABLES

CHAPTER 1: INTRODUCTION

While estimates vary, it is believed that approximately 20% of the world's population suffers from some type of nasal airway obstruction [1]. Chronic rhinitis affects 20 million Americans alone [2]. Additionally, more than 35 million Americans are plagued by seasonal allergic rhinitis. However, because many people believe that their symptoms are sinus related or due to persistent colds, the condition is considered to be under-diagnosed and may affect more than 25 million Americans [3].

Beyond the direct effects of these medical conditions, there are subsequent consequences related to nasal obstructions. Healthcare costs induced by allergic rhinitis in the United States are estimated to be approximately $4 billion per year [3], $6 billion in 1996 alone. Some of these costs are due to the 14.1 million physician office visits that are attributed to allergic rhinitis each year [4]. Recent studies have also shown that, on average, the yearly cost to treat an individual with chronic rhinitis is $1,000; overall costs exceed $15,000 [2].

The high prevalence of chronic and allergic rhinitis in the global population and the lofty monetary expenses that follow make finding a solution to the problem of nasal obstructions an important goal. Ideally, all people would be born free from nasal obstruction. However, realistically many people must endure surgery to improve their ease of breathing. A partial nasal turbinectomy can be performed as a possible solution to nasal obstruction.

Currently, many studies have been completed to examine the effects of nasal turbinectomies. However, because these experiments have results based heavily on patient perception and computer simulation, the results are inconclusive.

Therefore, the goal of this project was to use physical models of pre and post operation models of human nasal cavities to measure airflow conditions before and after a nasal turbinectomy as well as to test the quasi-steady assumption currently made in most tests. In order to obtain these results, we used enlarged models of the nasal cavity through which we pulled water flow. The breathing frequency, volumetric flow rate, and pressure were scaled appropriately to account for the large size of the model and the use of water. We then measured trans-nasal pressure and flow. Using these large sized models and water as the fluid allowed us to view the streamlines by injecting dye into the flow and document them with publication quality photos.

The data collected in this project can be used to improve the procedure of future research projects and to provide preliminary data supporting the quasi-steady assumption.

CHAPTER 2: LITERATURE REVIEW

In order to complete our objectives and present our results, it is necessary to research and understand some background information in particular fields. The following chapter discusses nasal anatomy and functions, the process of a nasal turbinectomy, previous study regarding nasal turbinectomies, and the elements of fluid dynamics relevant to this project.

NASAL ANATOMY AND FUNCTION

The nasal cavity contains the smell organs and also provides a passageway for air during respiration. Within the nasal cavity, air is warmed and filtered before joining the throat and trachea. The cavity is primarily used during at-rest respiration, because active respiration requires opening of the mouth to increase air-flow volume, thus routing airflow away from the nose [5]. The focus of this study will be the nasal cavity, specifically the structures within and how they influence airflow. This section will describe the anatomy of the nose, knowledge that is essential to provide background for this study.

The nasal cavity is the area between the tip of the nose, or nasal vestibule, and the throat, through which air flows during at-rest respiration. The nasal cavity and basic anatomy of the airflow pathway can be seen in Figure 1.

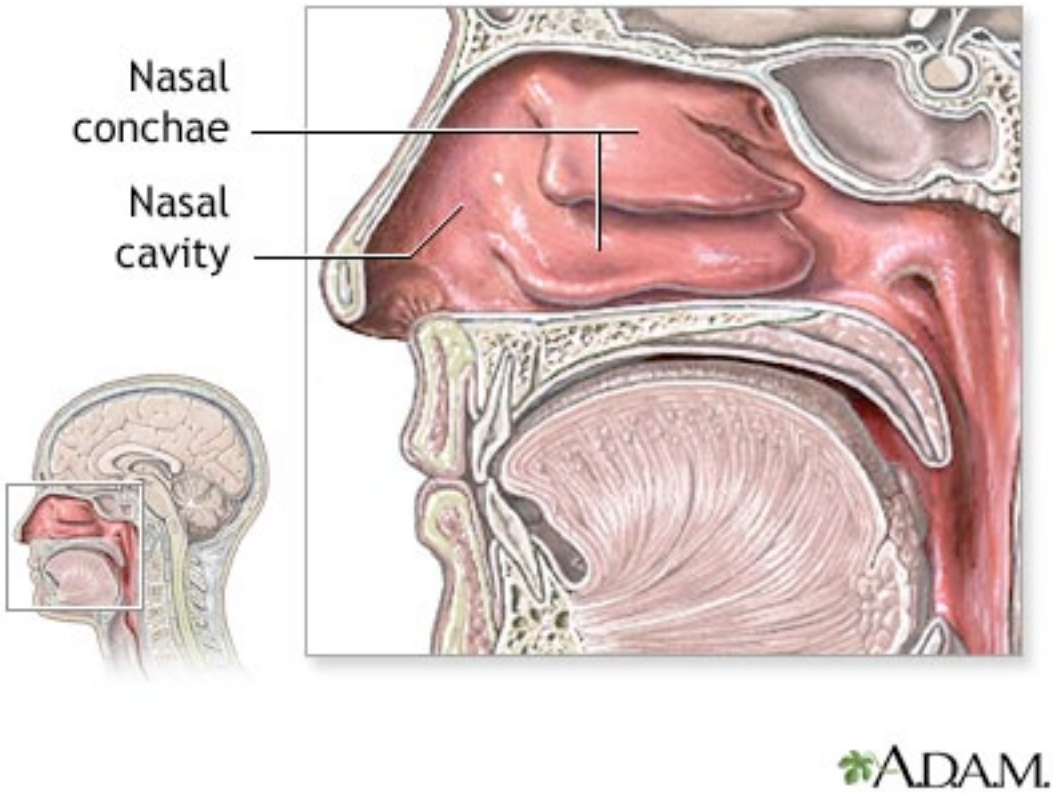

Figure 1: Diagram of the Nasal Cavity

http://www.nlm.nih.gov/medlineplus/ency/images/ency/fullsize/9657.jpg

This cavity contains variable surfaces composed of tissue, bone and hair. The rough surfaces cause swirling and turbulence during breathing, which affects airflow [6]. The first and most easily identifiable of these features is the cartilaginous septum, which divides airflow in two paths – the nostrils.

Within the nasal cavity there are four segments that limit airflow: the nasal valves. Theses valves, formed by the protruding nasal conchae, are visible in Figure 2

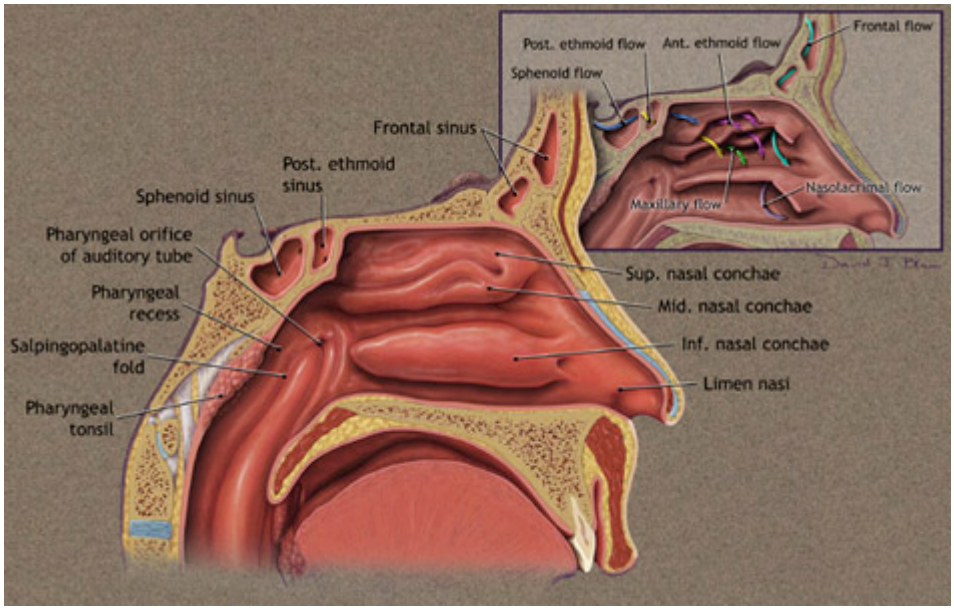

Figure 2: Nasal anatomy (detail)

http://www.blumdesign.com/portfolio_h/medical-illustration/05.html

The nasal valves are blamed for a high percentage of all airflow restrictions [7]. The four segments, from anterior to posterior, are the external valve, the septal valve, the internal valve, and the inferior turbinates [5]. The cross-sectional area of the nasal cavity gradually decreases throughout the nasal valves, up to the internal valve, where the cross-section is unlike the rest of the nasal cavity. This section, the main nasal airway, contains three sections of bone-supported fleshy ridges referred to as turbinates, or conchae, on the sides of the cavity.

The three sections of turbinates are lower, middle and upper as in Figure 3.

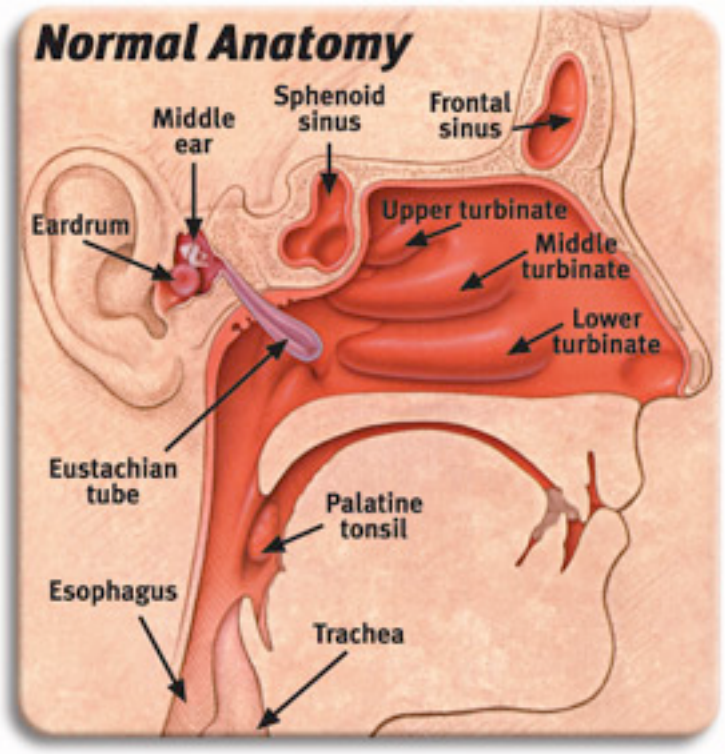

Figure 3: Normal turbinate anatomy within nasal cavity

http://www.unimedprod.com/images/NormalAnatomy_USA.jpg

They are sometimes referred to as the inferior, middle and superior as in Figure 4.

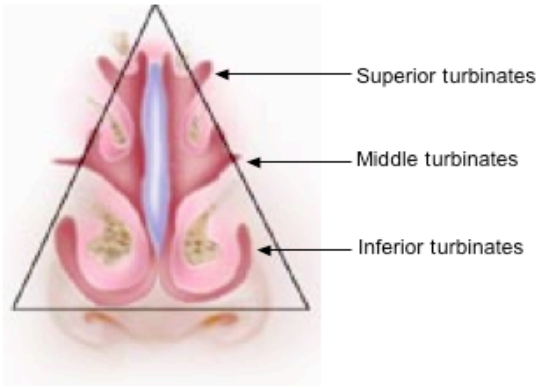

Figure 4: Turbinate structure

http://www.nose.co.za/images/illustrations/turbinate_surgery.jpg

The varying cross-sectional areas of these turbinates contribute to the complexity of airflow through the nasal cavity. The dimensions of the nasal cavity in the turbinate area are about 40 mm high, 1-3 mm wide, and approximately 60 mm deep [8].

The separate passages of airflow rejoin after the inferior turbinate and enter the nasopharynx, the final region of the nasal cavity. Airflow in the nasopharynx proceeds to the pharynx, which is considered a part of the throat. The cross-sectional area of the nasal cavity in the nasopharynx is greater than in the turbinates and so it is not considered the cause of airflow restrictions.

The turbinates redirect air into certain nasal passages depending on function. The superior turbinate, which contains the olfactory nerve, redirects air for scent processing and also circulates air to moisturize and heat it [6]. Patients with breathing difficulties whose noses are to blame are sometimes referred to otolaryngolic surgeons who perform nasal turbinectomies. This procedure entails partial or total removal of one or more of the turbinates [7]. However, many patients end up having recurring nasal complications after this surgery because it is difficult for surgeons to know how much nasal tissue to remove in order to maximize airflow.

The region of the nasal cavity above the superior turbinate is believed to be vestigial in humans and only around 14% of inspired air reaches the area [6]. Research suggests that removal of the middle turbinate causes few complications in patients. Patients receiving the treatment displayed significant decreases in nasal resistance and reported easier breathing [7]. The inferior turbinate has the most drastic effect on the flow of air through the turbinates since it creates a bottleneck where air is forced through the smallest cross-sectional area in the nasal passage.

Breathing

In order for a researcher to successfully mimic breathing, as is desired in this study, several functional measurement parameters of breathing mechanics are of great

importance. Important data include the tidal volume, its derivative with respect to time (the rate of volumetric flow), and changes in pressure. Figure 5 summarizes one researcher's findings of typical respiratory variables for normal, healthy adults [9].

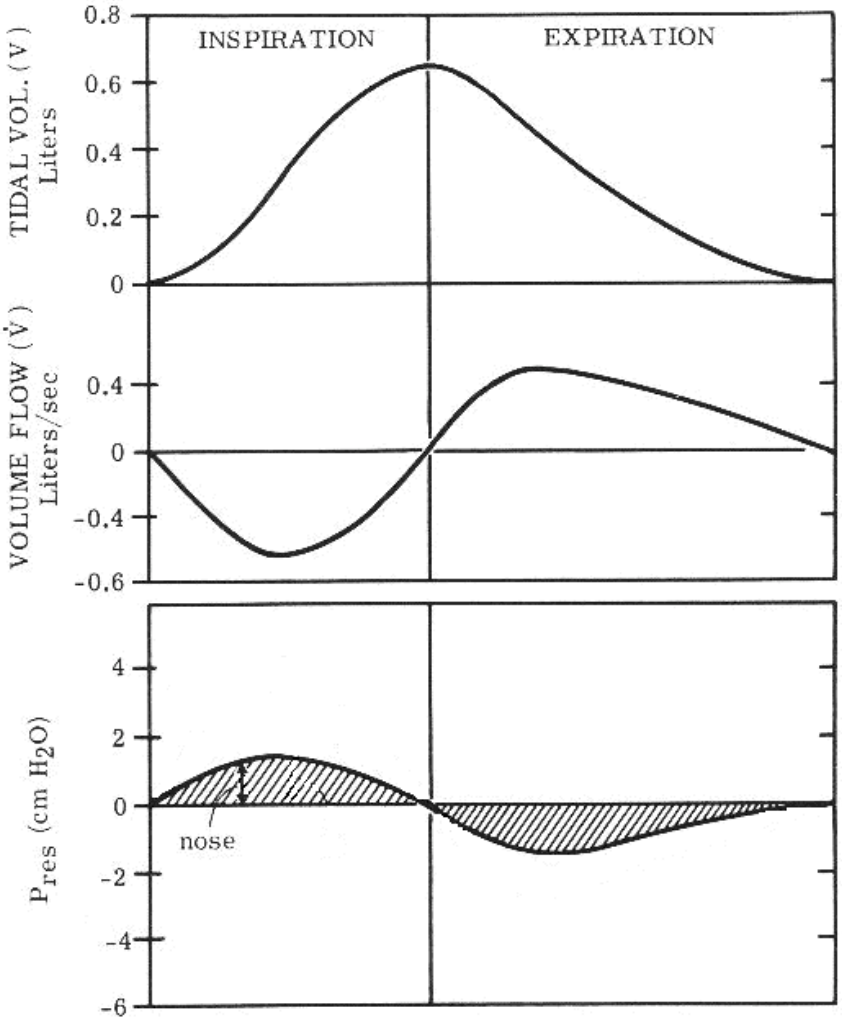

Figure 5: Tidal volume versus time, volumetric flow rate, and pressure charts [9]

The hypothesis that resistance to flow during inhalation is greater is supported by comparing the magnitudes of maximum inhalation and exhalation pressures (1.7 cm H_2O and 1.5 cm H_2O, respectively).

In order to properly mimic breathing it is also important to understand breathing parameters. Humans are variable and so are breathing rates. Table 1 displays breathing rates for different age groups in breaths per minute (BPM).

Table 1: Typical Breathing Rates [9]

Typical Breathing Rates		
	Low (BPM)	High (BPM)
Adult	12	20
Teenager	16	25
Preschool	20	30
Infants	20	40
Newborns	44	

An understanding of breathing mechanics, breathing rates and tidal volumes will be essential in modeling nasal airflow. Similarly, knowledge of the anatomy and topography of surfaces is necessary to model this process. By converting these anatomical systems into mathematical expressions it will be possible to model airflow and therefore predict and possibly maximize the success of turbinectomy procedures.

The following chart, Figure 6, illustrates typical lung volumes for healthy adults. This chart provided information for calibrating the device motor for this project. Knowledge of the correct volumes, rates and pressures was essential for modeling the breathing curve. The project device is meant to measure normal nasal breathing and is meant to follow the “normal inspiration” portion of Figure 6, approximately 2.30 to 2.80 liters of air.

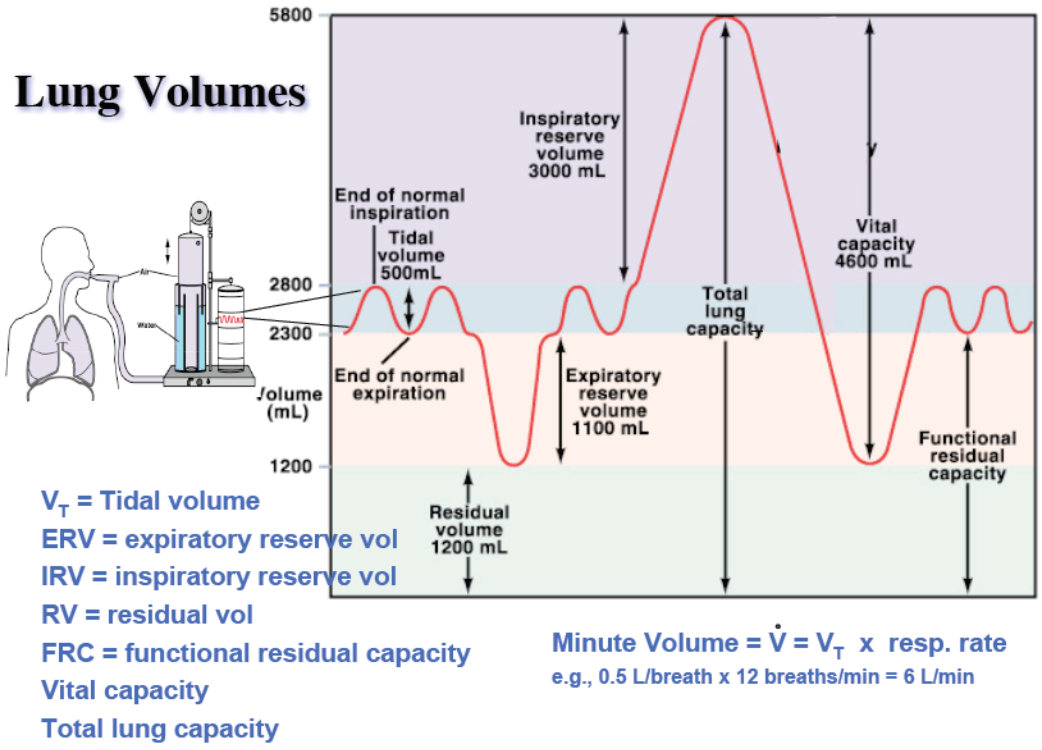

Figure 6: Lung Volumes over Breathing Cycle

http://mcb.berkeley.edu/courses/mcb136/topic/Respiration/SlideSet1/Resp1.pdf

DESCRIPTION OF A NASAL TURBINECTOMY

Twenty percent of the world's population suffers from some type of nasal airway obstruction; the most common being hypertrophied inferior turbinates [1]. Caused by either allergic or vasomotor rhinitis, nasal airway obstruction results in sleep apnea or snoring [10]. In many cases, the airway is obstructed due to a "deviated nasal septum, swelling of the turbinate due to allergy, chronic inflammation, or chronic sinusitis, nasal polyps or other tumor obstructing the nose, or the swelling of the adenoids" [11].

A turbinectomy, the surgical removal or partial removal of an abnormally enlarged turbinate from the inside of the nose to improve breathing [12], may vary from person to person depending on the particular anatomy of the nose. This procedure may be performed as an outpatient procedure where the surgeon can remove only bone or both bone and soft tissue from within the nose [1].

One of the most common methods of completing a turbinectomy involves using a microdebrider, a tiny, high-speed device that shaves soft tissue [11]. With this process, the microdebrider is inserted through a tiny incision in the nose. Using a computer tomography guided imaging system, the surgeon is able to quickly and accurately remove the desired tissue while leaving the remaining tissue undisturbed [11].

There are many benefits for patients who choose to undergo a turbinectomy surgery. These benefits include improved nasal airway passages, improvement in symptoms such as nasal discharge, an improvement in the frequency of sneezing, and an improvement in recurrent rhino-sinusitis [1].

PREVIOUS STUDY THROUGH COMPUTER SIMULATION, EXPERIMENTAL DATA, AND CASE STUDIES

In order to obtain the objectives of this project, it is necessary to have a firm understanding of what has already been studied and what conclusions were reached. Special attention must be paid to references to the inferior turbinates as our study is specifically looking at flow characteristics pre and post turbinectomy.

Similar objectives can be found between studies. In general, studies regarding nasal airflow are looking to gain a better understanding of the flow characteristics and to

evaluate the effect of physiological changes to the nasal passages. Even with similar objectives, the study of airflow through the human nasal passages can be separated into two main groups: computer simulated and experimental.

Computer simulations are desirable as they may help to serve as a guide for surgical planning in the future [13]. Studies using computer simulation have been based on finite element meshes taken from both CAT scans and MRI images, which were later analyzed using the Navier-Stokes and continuity equations. One problem with this method is the assumptions that are used. There is debate about the assumption of laminar flow and steady flow.

When looking at the experimental studies, most use scaled up models of the nasal passages. However, the production of the models can be very different. The models have been produced using molds of cadavers, rapid prototyping techniques, Styrofoam cut outs based on CAT scans, and Plexiglas plates based on MRI images [15]. One difficulty faced by experimental studies on exact models is the small size of the nasal passages such that measuring air speed, pressure or other physical parameters becomes impossible without disrupting the airflow patterns. According to two different studies, laminar flow exists in the nasal cavity [8] [15].

The only methods for obtaining information from exact scale models so far have been limited to videotapes and direct observation, which cannot yield numerical data. Therefore, the models are often scaled up to allow for the introduction of pressure transducers or other measurement devices without interference with the airflow patterns. There is some debate about the accuracy of scaling up the models of the nasal cavity [14].

With regards to inferior turbinate reduction, several conclusions were reached. Simulated inferior turbinate reduction reduced the pressure drop along the nasal passages with airflow minimally affected in some spots in the passages [13]. Simmen et al. made the conclusion that partial inferior turbinectomy improves airflow resistance in a congested nose. However, excessive surgery can lead to mucosal drying and crusting particularly at the head of the inferior turbinate.

One challenge to the study of nasal airflow has been the need to use plug flow not pulled flow to induce flow. Plug flow is defined such that the velocity of air entering the nose is laminar perpendicular to the nasal inlet and that the velocity does not vary across the diameter of the inlet [13]. Pulled flow would more closely resemble human breathing.

Case studies also provide some insight into the effects of turbinectomy surgeries. A randomized clinical trial was performed in order to evaluate the effectiveness of nasal turbinectomies in patients with anterior septal deviations [16]. The study involved 26 patients, 21 men and 5 women, averaging 31 years of age. The subjects were divided randomly into two groups. One surgeon performed the surgeries on all the patients. For one group, only a septal surgery was performed. For the other group, a septal surgery and a turbinectomy were performed. In order to gauge the difference before and after the surgery, the patients completed a questionnaire and carried out active anterior rhinometry.

The study results showed no significant difference in the patients who had the septal surgery and those who had the additional turbinectomy. Because of this, the study

does not suggest that the turbinectomy provides any additional reduction of resistance to airflow through the nasal passages [16].

Another study regarding the benefits of nasal turbinectomies was conducted on patients with chronic sinusitis. In this study, functional endoscopic surgeries and partial middle turbinectomies were completed for each of the patients, who ranged from 8 to 70 years old and averaged 39.9 years old. The nasal functions that were measured pre- and post-operation in each patient were airflow and resistance [7].

Based on the airflow and resistance measurements, the partial middle turbinectomy did not impair these nasal functions [7]. The partial middle turbinectomy improved nasal function in the small group of patients who participated in this study [7]. However, many of the results gained through various turbinectomy studies are unreliable.

For instance, a study showed favorable results, but they were disputable [10]. In this study, 118 patients, 72 women and 46 men averaging 36.4 years old, were examined before and up to 5 years after the surgery. Seventy patients were treated with a CO_2 laser and 48 with an Nd:YAG. Each of the turbinectomies performed in this study were executed to relieve obstruction to nasal airflow [10].

Rhinometry and a questionnaire were done pre- and post-operation to gauge the effects of the surgeries completed. Both sets of surgeries showed little or no negative side effects, and although the results showed that the laser surgery had better long lasting effects, both sets of surgeries were considered successful. However the results are disputable because the rhinomanometry data only showed a 58% correlation with the patient feedback. So the success rating was based only on patient perception and not the rhinomanometry readings [10].

These debatable results show that more study needs to be done regarding the technical effects of nasal turbinectomies in order to confirm the positive effects of the surgery.

BASIC FLUID DYNAMICS

The purpose of this section is to provide the definitions of flow separation, turbulent versus laminar flow, and the necessary flow parameters, which are integral to completing the project objectives.

In order to observe the flow separation that occurs in this experiment, one must understand what it is they are looking for. As with all fluid flow, when air flows though the nasal passages, friction causes the fluid in contact with the boundary surfaces to become static. The particles close to the boundary surfaces have a smaller velocity than that of the free stream. This velocity gradient creates a boundary layer. If there is an adverse pressure gradient across that boundary layer, flow separation will occur [17]. At this point, vortices form along the flow containment surfaces (see Figure 7).

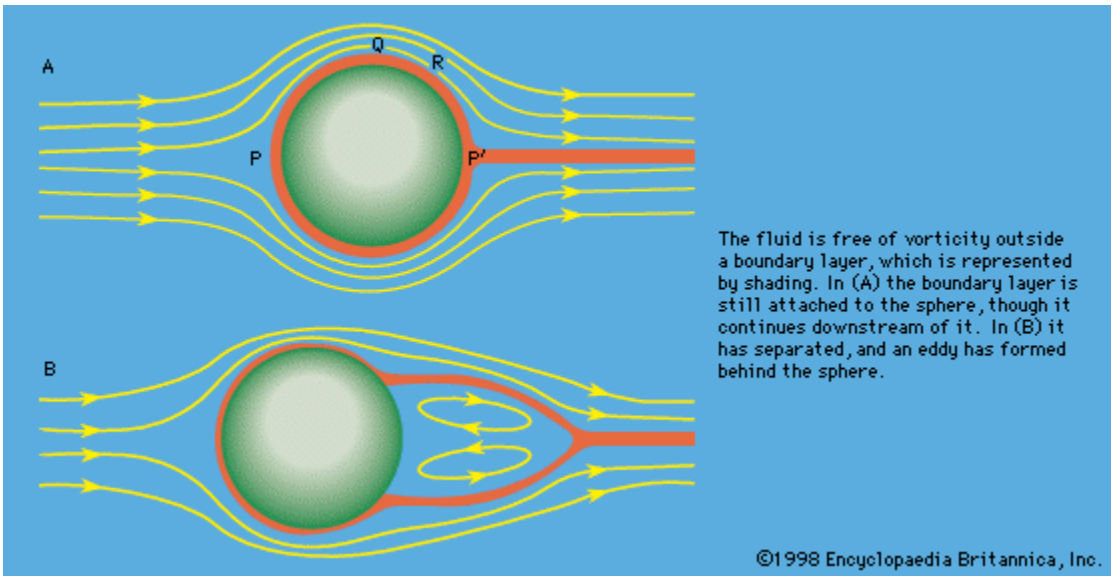

Figure 7: Flow Separation

Visually, laminar flow is characterized by fluid particles that move in smooth layers, while turbulent flow consists of fluid particles that mix rapidly as they move due to randomly changing velocity over time [18]. In the case of airflow through nasal passages, turbulent flow creates higher resistance, which increases difficulty while breathing. However, it allows for increased heat and mass transfer.

One indication of whether it is laminar or turbulent is the Reynolds number (see Equation 1); for straight pipeflow, the flow will become turbulent for Reynolds greater than 2300-4000. However, because of the unusual dimensions of the nasal cavity, turbulent flow is distinguished from laminar flow through the mixing and local perturbations of velocity with time.

Equation 1: Reynolds Number

$$\mathrm{Re}_d = \frac{4 \times Q}{\pi \times d \times \nu}$$

Here Q is the volumetric flow rate, d is the effective diameter of the nasal passage, and ν is the kinematic viscosity.

In this experiment, the dimensionless parameters used to scale the flow conditions being modeled are the Reynolds and Womersley numbers. These parameters were selected because they are typically used to characterize flow in biological systems with pulsatile flow [19]. Similar studies support this choice [20] [21] [22] [23].

Using the known flow rate of air through the nasal cavity, the Reynolds number can be used to find the appropriate flow rate for the enlarged model using water to represent air. The Womersley number (see Equation 2), the ratio of unsteady forces to viscous forces, is used in the same way to find the appropriate scaled value of the breathing frequency. In using these equations to characterize the flow, an enlarged model that uses water to simulate air can accurately portray airflow through the nasal cavity.

Equation 2: Womersley Number

$$\alpha = R \times \sqrt{\frac{\omega}{\nu}}$$

Here, ω is the breathing frequency and R is the reference length, the radius in this case.

CHAPTER 3: PROJECT APPROACH

The objective of this project was to improve the understanding of unsteady flow through and the pressure drop across the nasal cavity. As established in the previously mentioned literature, there are many questions about the accuracy of computer simulations due to the necessary assumption of either laminar or turbulent flow as well as the inconsistencies between the results attained using these simulations and those attained through physical measurements in humans. Therefore, in order to fulfill the aforementioned project objective, we developed the following project specifications.

First, we needed to obtain a model that accurately portrays the intricate details of the nasal passage. This is important because any results obtained would only the acceptable and useful if the model of the nose is accurate enough to truly represent human breathing. We then needed to supply the model of the nasal cavity with flow that would represent the human breathing pattern. Although experiments have been done in the past that collect data using constant flowrates, these do not address the unsteady nature of human breathing. Due to the low Strouhal number, researchers have assumed quasi-steady flow, and we wish to evaluate that assumption. Therefore, it is very important that the flow is an accurate depiction of human breathing.

Once the physical system has been produced, we needed to use pressure transducers that could accurately measure the pressure drop across the nasal cavity with +/- 5% error as specified by our project sponsor, Dr. David Wexler. In order to address the second project objective, we used a transparent model of the nasal cavity and created streaklines in the flow that could be captured in publication quality photographs and

video. This allowed us to acquire data regarding the level of turbulence as well as vortex development and flow distribution in the nasal cavity for normal human nasal breathing.

CHAPTER 4: DESIGN

To complete the specific aims of this project, a mechanism needed to be designed to create flow through a model nose that mimics that of the actual human breathing cycle. The following chapter details the necessary design specifications for this mechanism and the steps taken to finalize and create the design.

SPECIFICATIONS

To obtain the desired pressure readings and flow visualizations, the following specifications need to be met:

1. A model nose that accurately depicts the intricacies of the human nasal cavity
2. A fluid that can hold dye well enough to create streaklines showing flow paths
3. Induced flow scaled to represent the human breathing flow rate and frequency with repeatability
4. Total cost should be approximately $600
5. The pieces of the system must be manufacturable and durable given the timeline of the project
6. The final system must be user-friendly to allow for timely testing
7. The setup must allow for pressure measurements

ALTERNATIVE DESIGNS, FEASIBILITY, & DECISIONS

The first step necessary to obtain the desired outcomes of this project is to create the physical setup for data collection. To do this, our group obtained models of a patient nose pre- and post-turbinectomy from an MRI. Due to the ease of use and its ability to hold dye well, we chose water for our working fluid. We then needed to build a mechanism to create flow through the model nasal passage. We brainstormed multiple possible set-ups to create this flow.

The first option we explored was a piston CAM follower mechanism, which would create flow through the model to represent the breathing cycle. The CAM would be designed with an appropriate shape to mimic actual breathing rates. A sketch of this option is shown in Figure 8. Some possible problems associated with this model are the large piston necessary to create the appropriate flow volume as well as the likely mechanical noise and oscillations due to the spring, which would be used to return the piston. However, this positive aspect is that it is commonly used; therefore, the mechanism is well documented.

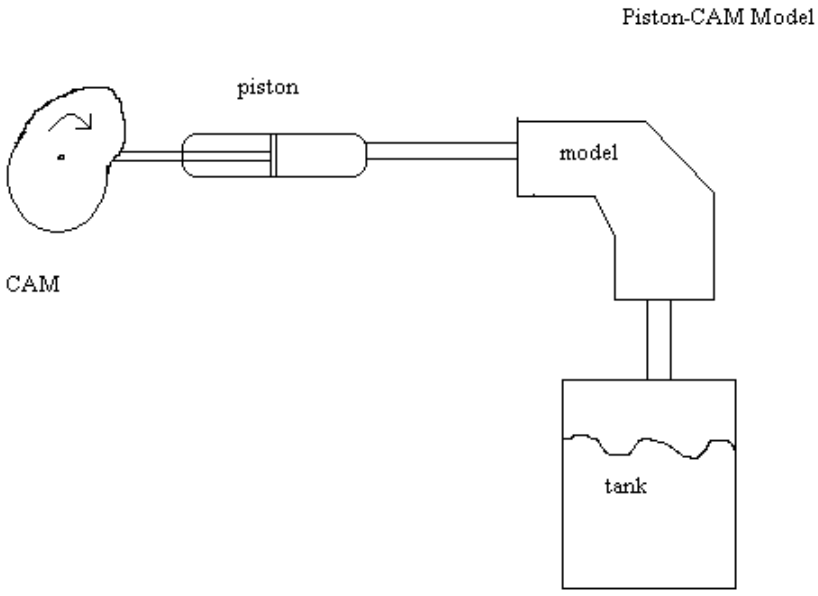

Figure 8: Piston-CAM Model

The next idea brainstormed was a system of pumps, valves, and reservoirs. In this system, which is shown in Figure 9, one pump and valve set would create flow from a reservoir to imitate inhalation and the other set would create expiration. The problem with this mechanism is that we would need pumps that we could program to pump

variable flow because we do not breathe in or out at a constant rate. We found limited resources for this type of pump.

We also considered a variable speed peristaltic and roller pumps for this purpose. However, we found that there were few to no pumps commercially available that would be able to perform the necessary task. The available pumps were not only not readily able to serve our purpose, but also very expensive.

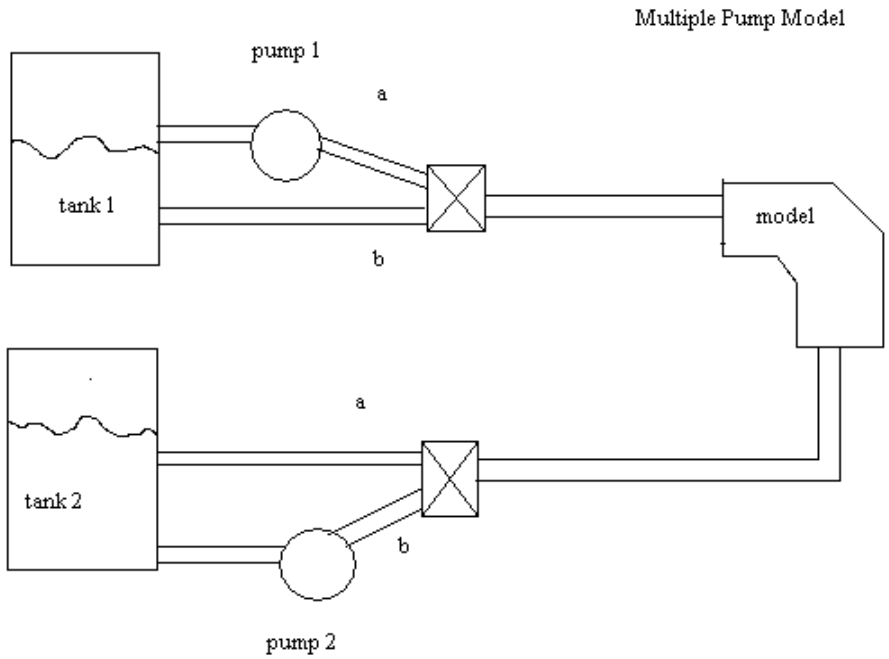

Figure 9: Multiple Pump Model

From the previously mentioned idea, we created and investigated a similar model that incorporated a solution to the problem of variable flow pumps. In this mechanism, which is shown in Figure 10, the system would use pressurized tanks instead of pumps. The system would consist of two reservoirs which would be sealed air tight. These would each be hooked up to one end of the model and a shared compressor. A valve would connect each tank to the compressor.

To create the flow, the compressor would force air into tank 1 while tank 2 was opened to the atmosphere. The pressure difference would force water through the model at the same rate as the air would be forced into tank 1. Then, to change direction, the valve would switch the airflow into tank 2 and open tank 1 to the air, creating a reversed flow. To control the volumetric flow rate, the compressor would be programmed to create pressure resulting in the same volumetric flow pattern as the breathing cycle.

This design, while inexpensive, was not found to be the most technically feasible. The ability to control the compressor accurately enough was not guaranteed, which could possibly result in a breathing pattern that would not correctly represent human breathing. This and the fact the flow would be pressure driven instead of the pressure being flow driven would make the viability of results questionable.

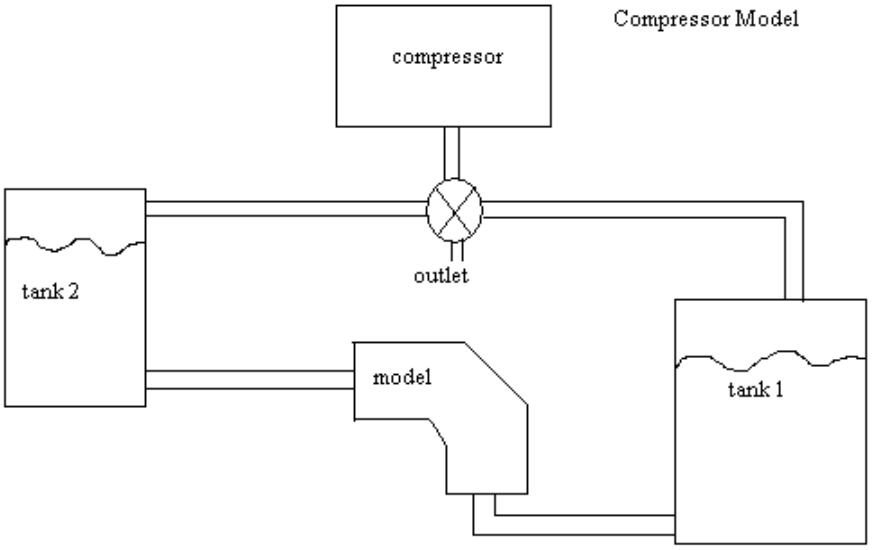

Figure 10: Compressor Model

Although we found that the type of pump necessary to create the desired flow was not commercially available, we did continue to pursue this idea. After exploring how a peristaltic pump drives flow, we found that we could build our own pump driven by a variable speed reversible motor not only to create variable flow rates, but also to eliminate the need for a second pump by reversing the flow direction. Shown in Figure 11. The only expenses were the motor, the aluminum that the pump pieces were machined from, and the tubing placed in the pump.

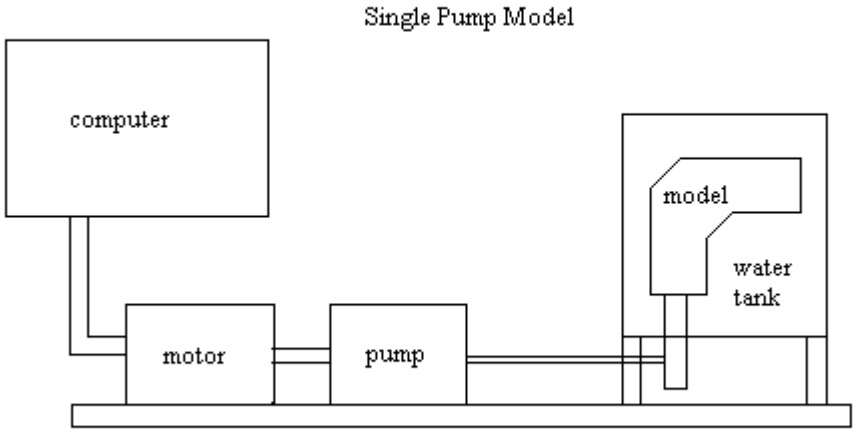

Figure 11: Custom-made peristaltic pump model

The customized pump design was the only design that would fulfill the necessary specifications previously listed. For this reason, we chose this design.

OPTIMIZATION

The pump was designed with dimensions that would not only maximize the motor's rate of rotation so that the motor would be able to run smoothly, but also make

the pump large enough to machine. The flow rate created by the pump is a function of the volume pumped per rotation of the pump rotor and the RPM of the motor as shown in Equation 3. This shows that in order to maximize the RPM of the motor, the volume pumped per rotation of the rotor was minimized. The rotor and rollers were sized initially based off of the size of the casing and the thickness of the fully compressed tubing. However, the rollers were then sized down through trial and error to find a size large enough to completely compress the tubing and small enough to minimize the torque on the motor.

Equation 3: Flowrate to RPM relation

$$Q = V_{cycle} \times RPM$$

In order to do this, we explored the options available for peristaltic pump tubing and found the most appropriate sized tubing for the RPM range of the motor, Masterflex L/S 16 tubing and dimensioned the rest of the pump based off of the dimensions of the tubing. These dimensions can be seen in mechanical drawings (see Figure 13, Figure 14, Figure 15, and Figure 16). The 36 V brushless DC motor (Anaheim Automation, BLWS234D-36V-4000) was chosen based off of the requirements of the ProMotion software package, the torque measurements, price, and availability.

To determine the torque required to turn the roller pump we attached the circular plate to the shaft running through the pump and rotated the shaft until just before there were two points of contact in the roller pump as shown in Figure 12.

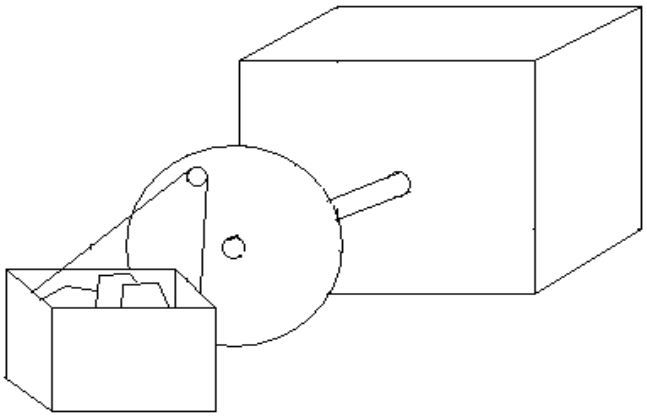

Figure 12: Torque Measurement Setup

The moment arm was calculated as the distance between the shaft and the screw on the outer perimeter of the plate (r=1.375 inches). A known amount of weight (F=28.145 oz) was added to the screw until the shaft rotated past the two contact points. Equation 4 was then used to determine the torque needed to rotate the pump. This information was used in determining the appropriate motor to use during the testing.

Equation 4: Torque Calculation

$\tau = F \times r$ = (28.145 oz)(1.375 inches) = 38.7 oz inches

MODELING

In order to begin the manufacturing process, we created computer models and drawings of the pump components using Pro-Engineer, which can be seen below in Figure 13, Figure 14, Figure 15 and Figure 16.

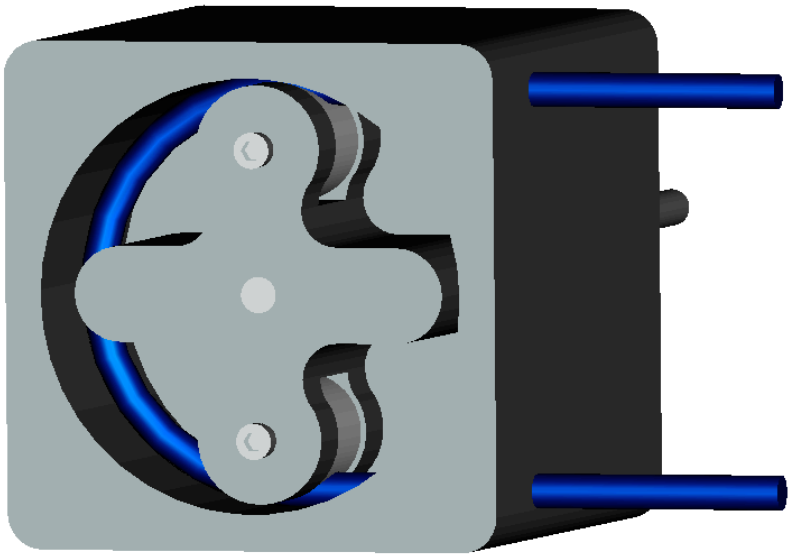

Figure 13: Pump Assembly Model

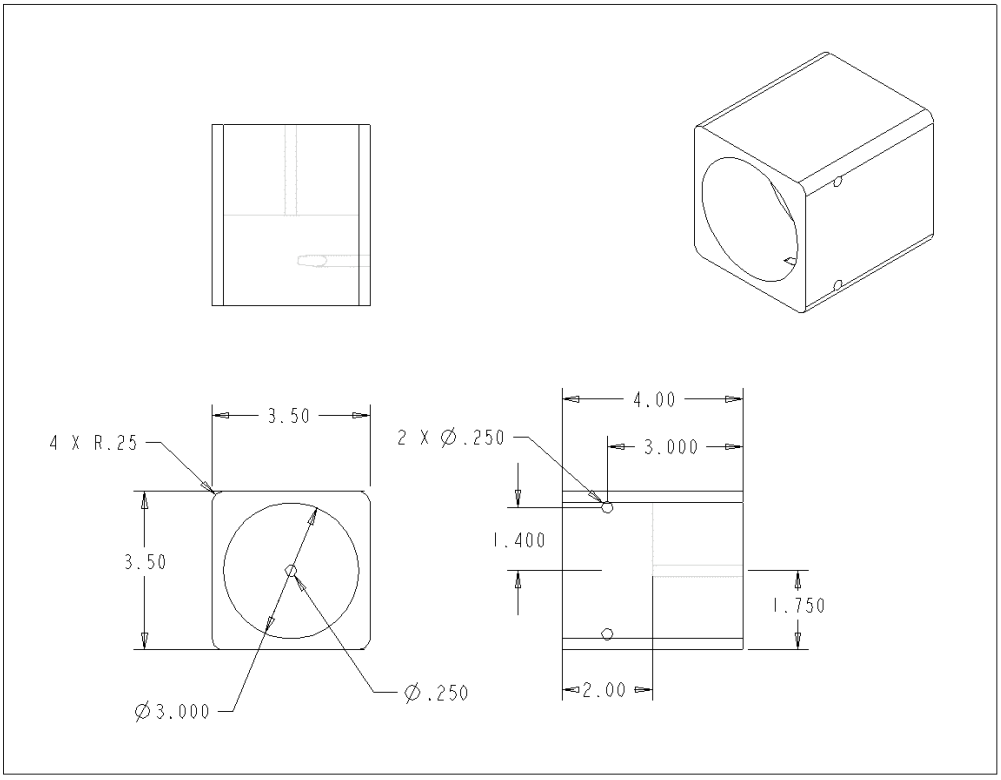

Figure 14: Casing Drawing

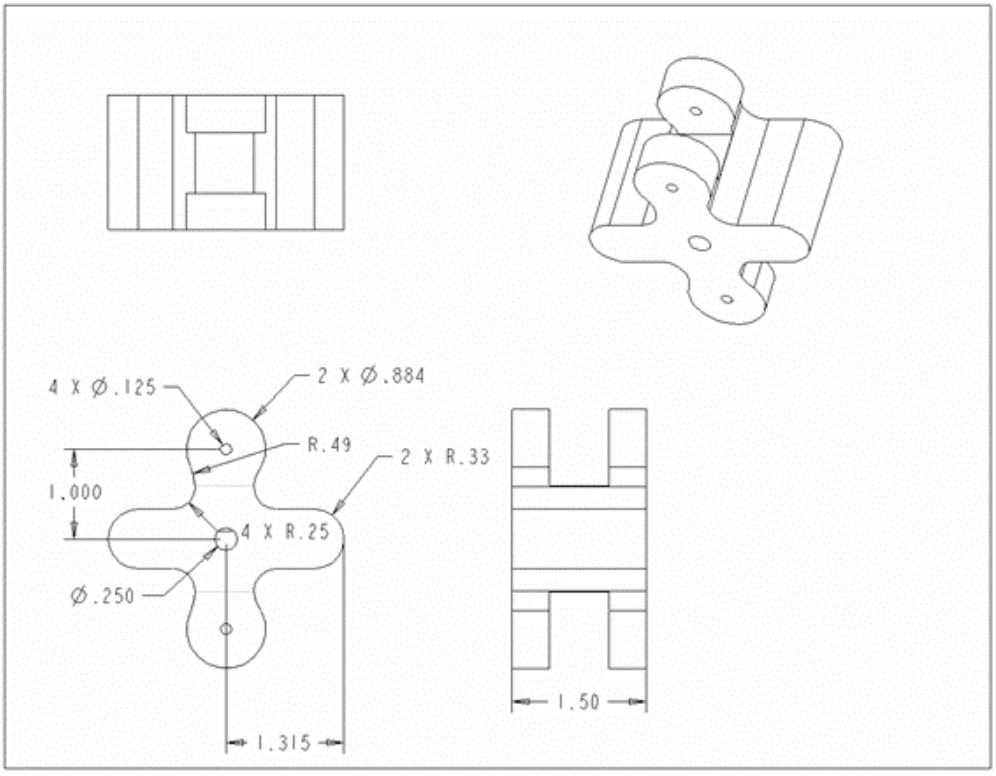

Figure 15: Rotor Drawing

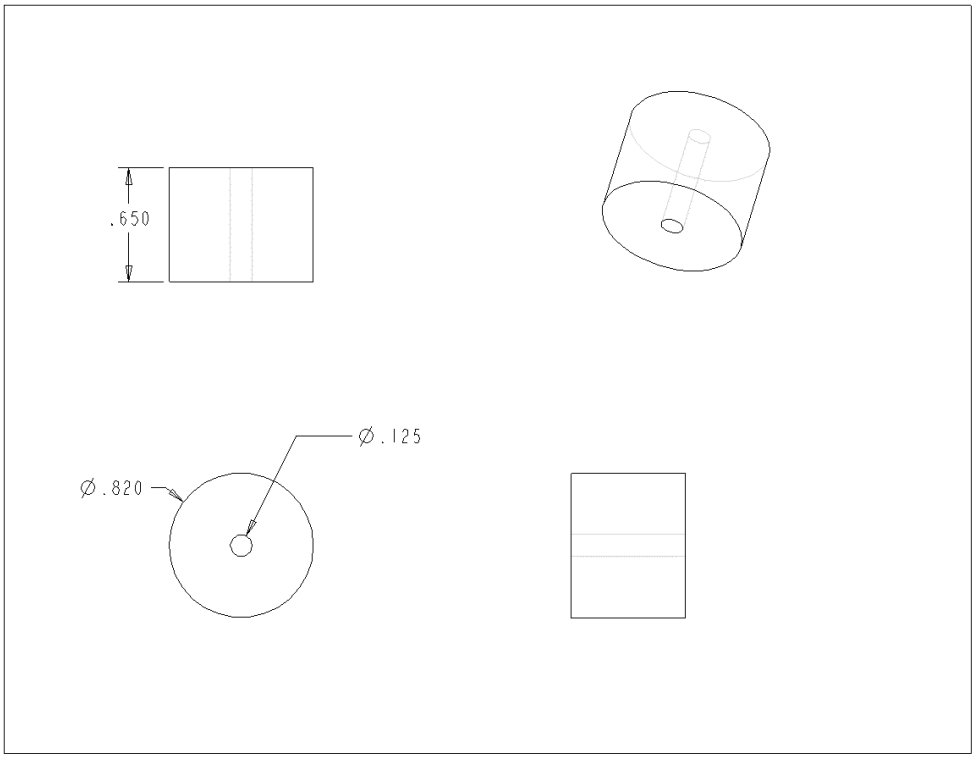

Figure 16: Roller Drawing

CHAPTER 5: METHODS

ESTABLISHING A BREATHING CURVE

The breathing curve was obtained from the Handbook of Physiology: Respiration [9]. For correct motor control, points were extrapolated from the breathing curve based on a breathing rate of 5 seconds/cycle. Individual points were marked along the curve and the coordinate values determined using a ratio of distances from the origin along the x-axis (time). The created the plot shown in Figure 17.

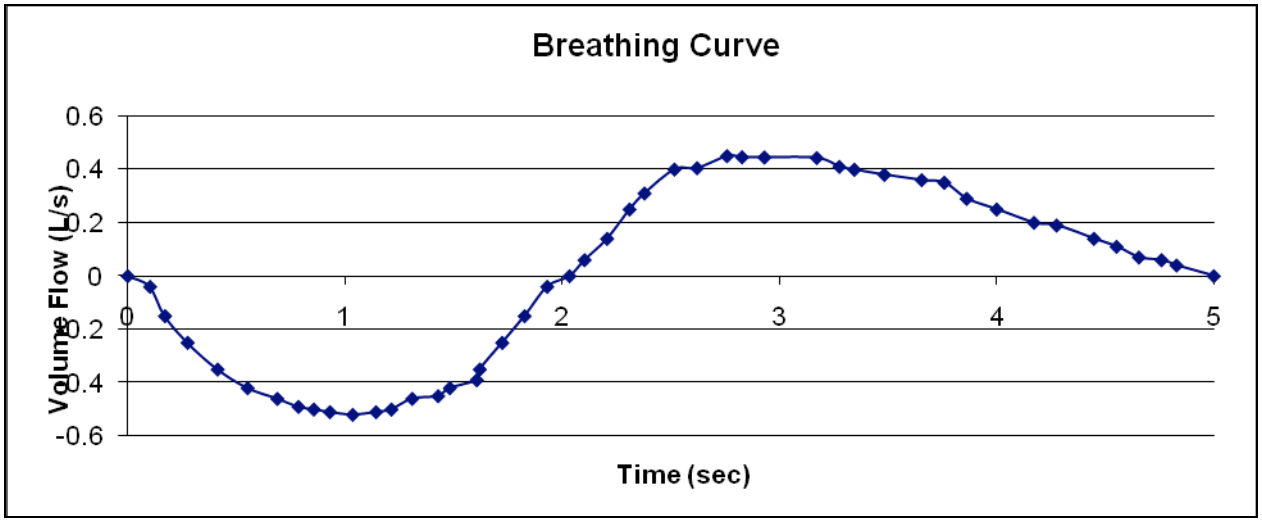

Figure 17: Breathing Curve for Normal Nose

However, our model is twice the size of a normal nose, and the working fluid is water instead of air. This means that the flow rate and time must be scaled appropriately to account for the change in size of the nasal cavity and in the viscosity of the fluid. To do this, we used dimensionless numbers to scale the flow. Through dimensional analysis, the Reynolds Number (see Equation 5) and the Womersley Number (see Equation 7) were used to scale the volumetric flow rate (see Equation 6) and frequency (see Equation 8) respectively (see Figure 18).

Equation 5: Reynolds Number

$$\mathrm{Re}_d = \frac{4 \times Q}{\pi \times d \times \nu}$$

Equation 6: Reynolds Number Dimensional Analysis

$$\frac{4 \times Q_N}{\pi \times d_N \times \nu_{Air}} = \frac{4 \times Q_M}{\pi \times d_M \times \nu_W}$$

Where,

Q_N = flow rate through normal nose
Q_M = flow rate through model nose

After completing the calculations, we found that:

$$Q_M = Q_N \times .12917$$

For details, see Appendix A.

Equation 7: Womersley Number

$$\alpha = R \times \sqrt{\frac{\omega}{\nu}}$$

Equation 8: Womersley Number Dimensional Analysis

$$R_N \times \sqrt{\frac{\omega_N}{\nu_{Air}}} = R_M \times \sqrt{\frac{\omega_M}{\nu_W}}$$

Where,

ω_N = normal breathing frequency
ω_M = model breathing frequency

After completing the calculations, we found that:

$$\omega_M = \omega_N \times .01615$$

For details, see Appendix A.

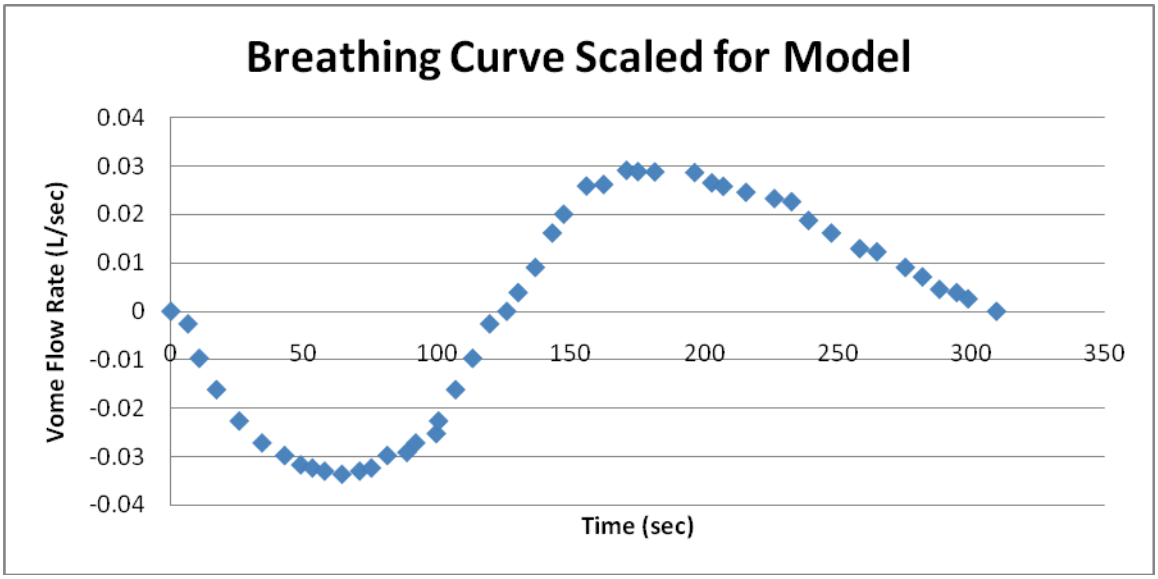

Figure 18: Scaled Breathing Curve

PROGRAMMING THE MOTOR

The pump motor was controlled using the ION Digital Drive from Performance Motion Devices Corporation. The motor was calibrated using the ProMotion 3.71 software package to provide a closer relationship between the desired position values and the actual position values. Tuning was important as it allowed the motor to more

accurately follow the desired motion profile. The motor was controlled based on the input of velocity values determined from the extrapolated points of the breathing curve, the scaling, and the relationship between the volumes pumped per turn of the motor (see Appendix B). The velocity was reset at a series of time points in the programming.

MANUFACTURING THE PUMP

The parts for the pump were machined using the Gibbs CAM 2007 software package and the previously prepared Pro Engineer drawings from above. The pump housing and rotor were constructed from aluminum alloy and the shaft from a stainless steel rod. The rollers were made from Delrin and affixed using shoulder bolts. When assembled, the pump was attached to the motor shaft with a flexible coupler.

COLLECTING PRESSURE DATA

Pressure readings were measured using a BIOPAC® Systems TSD160A Differential Pressure Transducer designed for low pressure readings in the range of +/- 2.5 cm H_2O. This transducer was chosen after predicting the approximate pressure readings expected. The pressure readings were estimated by scaling through dimensional analysis using Euler's Number (Equation 9 and Equation 10).

Equation 9: Euler's Number

$$E_u = \frac{P}{\rho \times V_F}$$

Equation 10: Euler's Number Dimensional Analysis

$$\frac{P_A}{\rho_A \times V_A^{\,2}} = \frac{P_W}{\rho_W \times V_W^{\,2}}$$

Where,

P_A = Pressure due to air
P_W = Pressure due to water

After completing the calculations, we found that:

$$P_W = .8722 \times P_A$$

For details, see Appendix A.

The TSD160A transducer was attached to a BIOPAC® DA100B Amplifier Module at a gain setting of 50. Low and high pass filters were turned off. The DA100B was connected to a UIM100A Interface Module attached to an MP100 Data Acquisition Module, also by BIOPAC®, which was attached via serial cable to a PC. Data acquired by the MP100 unit was viewed, recorded and filtered using BIOPAC® AcqKnowledge Software 3.2.6.

The first step necessary for pressure measurement was calibration of the system. Since the AcqKnowledge software recognizes the input from the TSD160A as Volts, these units must be expressed in more desirable units. This was accomplished using the Setup Channels>Calibrate Lag function in AcqKnowledge. The test system was completely set up at equilibrium (volume flow =0) and Cal 1 was clicked. This read the voltage being recorded at that point which was then associated with 0 cm of H2O. The value for Cal 2 was based on the value read by Cal 1, the gain, the reference voltage of the DA100B and the transducer specification for the relation between voltage and pressure. The software is designed to interpolate for all remaining values

The TSD160A Pressure Transducer was attached to the nasal models via two segments of standard 4 mm ID tubing. The tubing attached to the positive flow head was

connected to the lower end of the nasal model to a copper pipe designed to rest in the center of the throat of the model. The tube attached to the negative flow head was placed in the open nostril at the front of the model. Both of these tube locations also served as dye injection sites during the flow distribution experiments.

Once the system was fully connected and calibrated, a new AcqKnowledge file was started for each test, set to record readings for 10 minutes to avoid missing any valuable data. To record, the start button was clicked and readings began. The pump was run at the steady and unsteady state flows chosen for this experiment. The readings obtained were then duplicated and duplicate was filtered with a 1 Hz low pass filter to increase the signal to noise ratio. The filtered data was then unscaled using the waveform math function in AcqKnowledge with the output as a new waveform. . The resulting three waveforms were exported as text files to be analyzed in Microsoft Excel.

In Microsoft excel the data was averaged over 500 sample intervals to further smooth the curve and remove additional noise. In addition to averaging the samples it was also necessary to correct for drift in the transducer by averaging sections of the data from before and after the test where the pump was not in motion. This difference was then added/subtracted from the averaged values to account for it being the actual zero pressure recording. This resulted in a graph of pressure vs. time with normal and post turbinectomy steady and unsteady tests. The pressure data was also then correlated to the flows that would occur at the same time points to result in a pressure vs. flow graph.

VISUAL DATA RECORDING

For each model (pre and post-surgery) red water based food coloring was injected to during inhalation at each steady state flowrate chosen (6.42, 17.45, 25.23, and 32.28 cc/sec). In order to view streaklines at all points throughout the nasal cavity, dye was injected at both the anterior and posterior of the nostril opening. For the quasi-steady flow recordings, dye was injected at intervals along the breathing curve to match the steady state flowrates. The streaklines created with the dye were recorded using a 7.1 megapixel digital camera. Stills were then pulled from the video using Apple iMovie.

Once all of the video was collected, Logger Pro 3.4.5 was used to pull numerical data from the video. Each video was imported into Logger Pro, which then allowed the user to track and record the position of dye particles frame by frame. Using the model length as a reference, the program could then record the x and y velocity of the particle. These velocities were averaged to find the average velocity through the top (above the middle turbinate), middle (between the middle and lower turbinate), and lower (below the lower turbinate) paths through the nasal cavity (see Figure 4 for diagram of paths). Because of the timing of dye injections, some of the flowrates could not be collected.

CHAPTER 6: RESULTS

Through flow measurement, visual data recording, and pressure data recording, we obtained results regarding the true flowrate vs. time we obtained with our pump, the flow patterns created by that flow, and the pressure drop across the nasal cavity in a normal and post-surgery nasal cavity subjected to both unsteady and steady flow.

FLOW MEASUREMENTS

The flows obtained by our roller pump system are shown in Figure 19. This figure combines data collected at each motor velocity to show the actual breathing curve that was used when we collected our unsteady visual and pressure data.

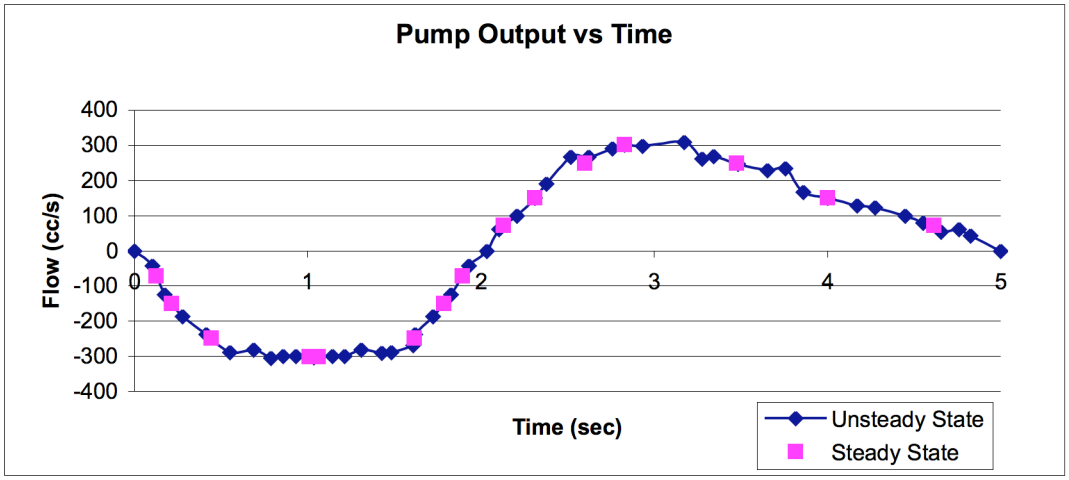

Figure 19: Pump Output vs. Time

FLOW VELOCITY DISTRIBUTIONS

The average velocities of the flow at each flowrate through the different paths in the nasal cavity are shown in Table 2 and Table 3. The tables show the velocities for steady tests and each time the flowrate appears in the unsteady cycle (1^{st} and 2^{nd}). The

complete set of data can be found in the Appendix. The images in Figure 20 are sample photos showing flow distribution at a flow of 6.4 cc/s before and after surgery at both steady and quasi-steady state. The rest of the images and the video can be found on the CD associated with this project.

Table 2: Flow Velocity Distribution Pre-Surgery

Flow	Flow Position	Steady Velocity (cm/s)	1st Unsteady Velocity (cm/s)	2nd Unsteady Velocity (cm/s)
6.4 (cc/s)	top	2 +/- 13.4%	3 +/- 30.2%	no data
	mid	3 +/- 13.2%	5 +/- 7.8%	4 +/- 18.5%
	bottom	3 +/- 2.4%	5 +/- 14.8%	3 +/- 12.3%
17.5 (cc/s)	top	5 +/- 7.5%	5 +/- 11.2%	no data
	mid	8 +/- 14.6%	7 +/- 16.1%	
	bottom	5 +/- 1.9%	5 +/- 10.3%	
25.2 (cc/s)	top	6 +/- 35.0%	4 +/- 13.6%	3 +/- 21.5%
	mid	8 +/- 14.0%	8 +/- 15.8%	5 +/- 15.7%
	bottom	7 +/- 14.1%	7 +/- 27.6%	6 +/- 8.3%
32.5 (cc/s)	top	11 +/- 11.05	3 +/- 10.5%	3 +/- 13.5%
	mid	13 +/- 15.6%	7 +/- 16.4%	7 +/- 19.6%
	bottom	11 +/- 27.1%	7 +/- 15.9%	7 +/- 15.4%

Table 3: Flow Velocity Distribution Post-Surgery

Flow	Flow Position	Steady Velocity (cm/s)	1st Unsteady Velocity (cm/s)	2nd Unsteady Velocity (cm/s)
6.4 (cc/s)	top	1 +/- 8.8%	2 +/- 23.7%	no data
	mid	2 +/- 23.3%	5 +/- 5.5%	4 +/- 6.8%
	bottom	2 +/- 18.8%	4 +/- 15.1%	3 +/- 9.1%
17.5 (cc/s)	top	3 +/- 19.3%	4 +/- 13.2%	no data
	mid	6 +/- 16.4%	6 +/- 11.5%	
	bottom	6 +/- 10.3%	4 +/- 8.2%	
25.2 (cc/s)	top	6 +/- 17.2%	5 +/- 9.6%	4 +/- 22.3%
	mid	8 +/- 18.3%	7 +/- 9.8%	5 +/- 11.8%
	bottom	6 +/- 10.5%	6 +/- 6.8%	4 +/- 17.1%
32.5 (cc/s)	top	6 +/- 7.5%	6 +/- 19.0%	5 +/- 6.7%
	mid	8 +/- 23.4%	8 +/- 14.8	7 +/- 9.3%
	bottom	7 +/- 2.1%	6 +/- 11.7%	5 +/- 11.0%

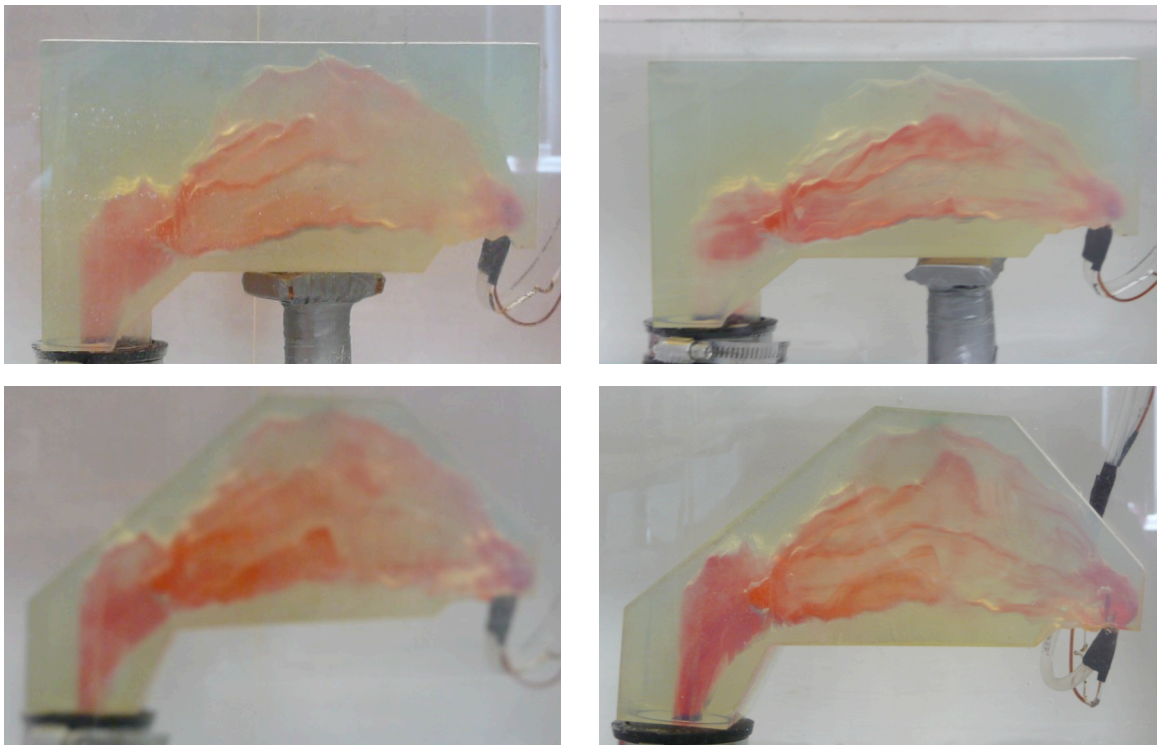

Figure 20: Dye Injection Video Capture at 6.4 cc/s Comparing Unsteady and Steady State (left and right) and Pre and Post Surgery (top and bottom)

PRESSURE DATA

The recorded pressure vs. time for steady and unsteady normal and post turbinectomy models is shown in Figure 21. The relation of the recorded pressures to the pump output is shown in Figure 22. The complete data can be found on the CD associated with this project.

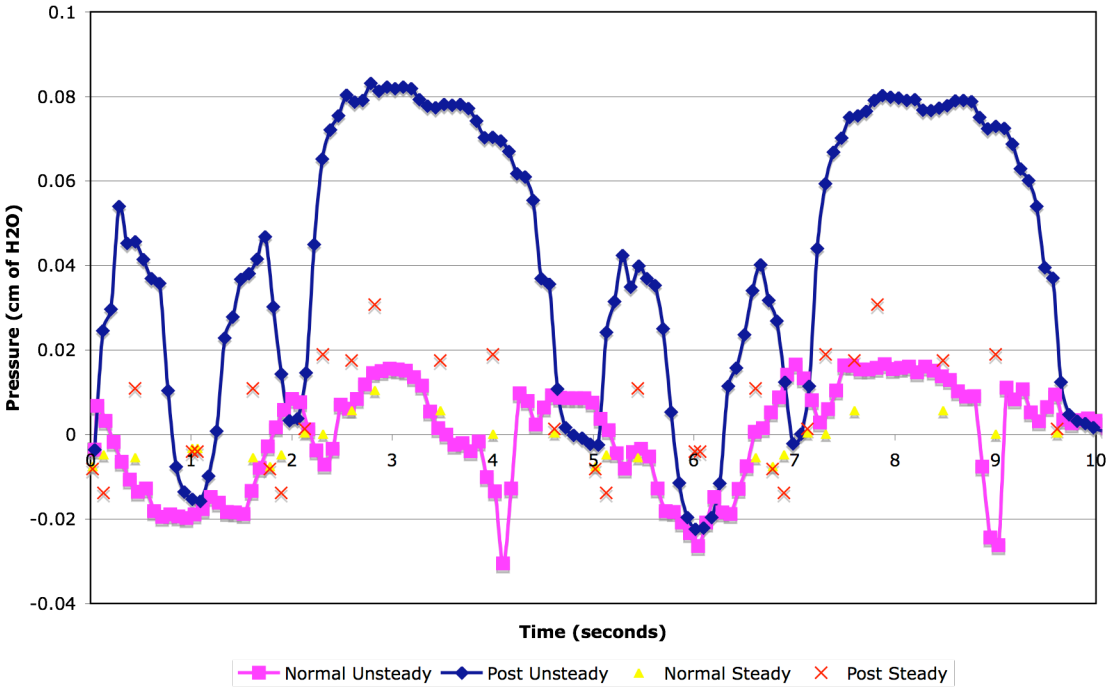

Figure 21: Pressure Curve for Normal Breathing in Both Nostrils

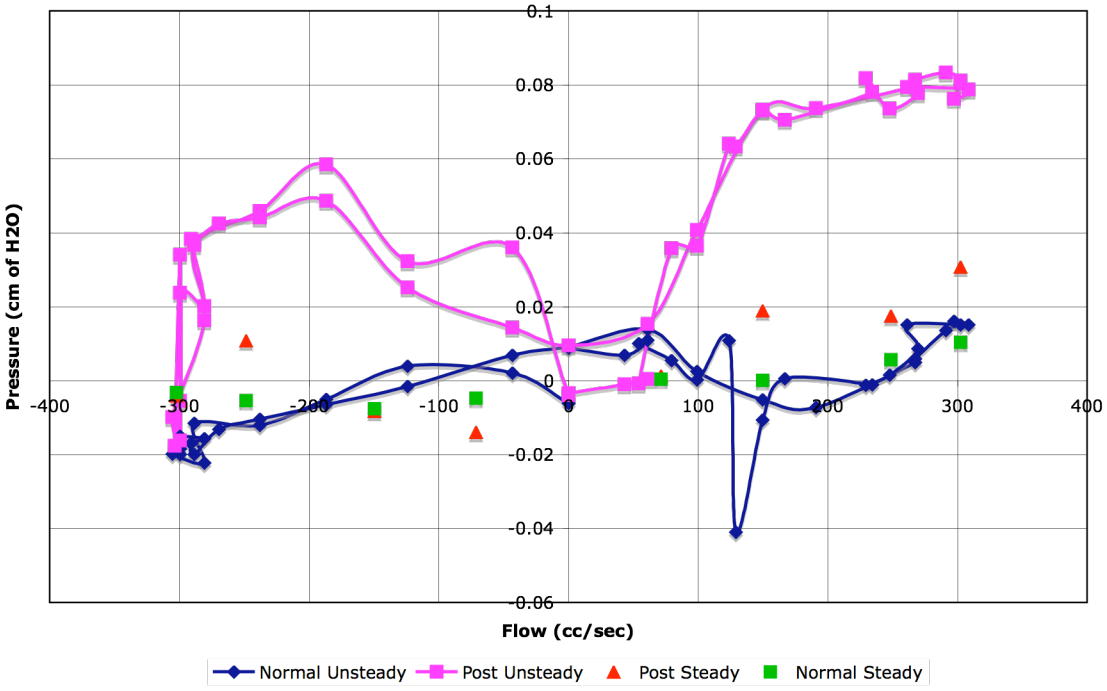

Figure 22: Pressure vs. Flow for Normal Breathing in Both Nostrils

CHAPTER 7: ANALYSIS & DISCUSSION

FLOW MEASUREMENTS

Analysis of the pump showed that there were several factors that contributed to the reduced functionality of this design. The freedom of movement of the shaft within the casing caused an increase in torque, limited control over flowrates, and decreased the durability of the pump. The movement of the shaft within the casing prevented full compression of the tubing while the rotor was rotating at high velocities. This resulted in limited control over the peak flowrates because the volume being pumped through the tubing with each rotation was lower than initially measured. As a result, the breathing curve actually produced could not reach the higher flow rates produced during normal breathing. The durability of the pump was less than satisfactory due to the problem with the shaft because during rotation the edges of the rotor were able to touch the inner wall of the casing, resulting in scratches and wear in the metal.

FLOW VELOCITY DISTRIBUTIONS

A comparison of the flow distribution velocities pre- and post-surgery for both the steady and unsteady assumptions showed that there is an evident decrease in the fluid velocity through all three sections of the nasal passage. This decrease in velocity is expected due to the increased cross sectional area of the passageways upon partial removal of the turbinates. The large percentage of error associated with many of the velocity readings makes the results showing decreased flow velocity post-surgery inconclusive. This is consistent with previous results [13] [16].

However, the large percent error may be due to the method by which the data was collected. Points were manually selected and tracked using the Logger Pro 3.4.5 software which makes it difficult to ensure that the same points in each video are being tracked. In addition, it is impossible to track every point through each section of the nasal passage, resulting in velocities that might not accurately represent the average velocity through a given section. As a result, the sum of the velocities through the three passages for a given flow rate is not consistent.

The still frames captured from the videos depicted a clear difference in flow between the pre- and post-surgery models. The pre-surgery model had concentrated flow through the inferior and middle turbinates, whereas the post-surgery model had a much more evenly distributed flow through the entire nasal cavity. It is believed that the removal of a section of soft tissue during a partial turbinectomy would account for this change in flow as the enlarged passageways allow for a more uniform flow distribution. It can be concluded from this that a partial turbinectomy does alter the flow distribution through the nasal cavity allowing more a more even distribution of flow.

Still frames were taken during the unsteady breathing cycle that corresponded with the steady flow rates that were also visualized. This allowed for a visual comparison of the steady and unsteady assumptions. No visual differences were detected between these images, indicating that any given point on the breathing curve can be visualized by the corresponding steady state flow at that point. This validates the quasi-steady state assumption that any point on the unsteady curve can be modeled by the steady state flow at that particular point.

PRESSURE ANALYSIS

The raw pressure data shows a very low signal to noise ratio defined as the mean divided by the standard deviation of the test) for the data recorded without a filter was between .926 and .152. These issues are partly due to noise generated by the operation of the pump and the sensitivity of the pressure transducer. Any motion of the transducer affected the pressure being recorded and since the range over which data was being recorded was very small the noise picked up was beyond a reasonable range.

To understand this vibration an FFT was computed for the signals, which showed peaks higher than 1 Hz. This was not consistent with the frequency expected for the pressure signal based on that the full cycle took 306 seconds. Therefore low pass filter was employed to remove much of the mechanical vibration. The data was also averaged over 500 sample sections as an additional way to remove noise.

The resultant data are shown in Figure 21 and Figure 22. There are some key issues with these final plots. For example the pressure recordings during inhalation (negative flow rates) should also be negative which is somewhat the case in the normal model but does not appear in the results from the post turbinectomy model. Also based on previous studies the magnitude of the post turbinectomy pressure measurements is not in a reasonable range of approximately 0.2 cm of H2O. In addition the fact that when the flow is zero the pressure difference should be zero is not present in our pressure recordings. Trends suggest that the normal data show correct trends and both the unsteady and steady data lie in the same range. The post turbinectomy data may suffer from both noise and inaccurate recalibration due to the height from inlet to outlet varying for the two models

CHAPTER 8: CONCLUSIONS AND RECOMMENDATIONS

The main conclusion of the data analysis is that the pump should be redesigned. The freedom of movement in the shaft caused increased torque, limited control over flow rates, and decreased durability.

It was also determined that the full breathing curve does not match the highest flows, but it works for lower flow rates up to almost 300 cc/s. This means that computer aided motor programming can be used to model a breathing curve, but in this case it was not the breathing curve desired. Instead, it corresponded to physiological volume and frequency data for a 15 year old female.

The vibrations of the motor caused significant noise in pressure readings, and the noise to data ratio was about 0.1. Future work should concentrate specifically on removing noise from sensitive transducer readings.

Preliminary results of the experiment appear to validate the quasi-steady state assumption. Future work into the analysis of the obtained data will reveal a better picture of the differences between pre and post partial turbinectomies as well as confirm this steady state assumption validation.

REFERENCES

1. Turbinectomy surgery [homepage on the Internet]. . 2007. Available from: http://www.sleepdisordersguide.com/sleepapnea/turbinectomy-surgery.html.

2. Bhattacharyya N, Dr. Symptom outcomes after endoscopic sinus surgery for chronic rhinosinusitis. Arch Otolaryngol Head Neck Surg. 2004 March 2004 [cited 09/28/07];130:329,330-333. Available from: http://archotol.ama-assn.org/cgi/reprint/130/3/329.pdf.

3. FAQ: Chronic nasal obstruction and enlarged turbinates [homepage on the Internet]. Gyrus ENT LLC. 2003 [cited 09/28/07]. Available from: http://www.somnoplasty.com/PatientTrack/FAQs/turbfaq.html.

4. Rhinitis and sinusitis statistics [homepage on the Internet]. American Academy of Allergy Asthma & Immunology. 2007 [cited 09/28/07]. Available from: http://www.aaaai.org/patients/gallery/rhinitissinusitis.asp?item=1a.

5. Lane AP. Nasal anatomy and physiology. Facial Plastic Surgery Clinics of North America. 2004;12:387-95.

6. Horschler, I., Ch. Brucker, W. Schroder, M. Meinke. Investigation of the impact of the geometry on the nose flow. European Journal of Mechanics B/Fluids. 2006;25:471-90.

7. Cook PR, Begegni A, Bryant WC, Davis WE. Effect of partial middle turbinectomy on nasal airflow and resistance. Otolaryngology--head and neck surgery : official journal of American Academy of Otolaryngology--head and neck surgery. 1995 Oct-1;113(4):413-9. Available from: http://www.sciencedirect.com/science?_ob=MImg&_imagekey=B6WP4-4HG68T6-F-1&_cdi=6980&_user=74021&_orig=search&_coverDate=10%2F31%2F1995&_sk=998869995&view=c&wchp=dGLbVtz-zSkWz&md5=f7c1f4d5dde2951c25845e3d178fc910&ie=/sdarticle.pdf.

8. Keyhani K, Scherer PW, Mozell MM. Numerical simulation of airflow in the human nasal cavity. J Biomech Eng. 1995 Nov-1;117(4):429-41.

9. Fenn, W.O., and Rahn, H. Handbook of Physiology: Respiration. Washington: American Physiological Society, 1964.

10. Lippert BM, Werner JA. Long-term results after laser turbinectomy. Lasers Surg Med. 1998 Jan-1;22(2):126-34. Available from: http://www3.interscience.wiley.com/cgi-bin/fulltext/34096/PDFSTART?CRETRY=1&SRETRY=0.

11. Turbinectomy [homepage on the Internet]. . 2002. Available from: http://www.entcolumbia.org/turbin.htm.

12. Nasal airway surgery and surgical instructions [homepage on the Internet]. . 2002 April 14, 2002. Available from: http://www.medicinenet.com/script/main/art.asp?articlekey=6248&pf=38&page=1.

13. Wexler D, Segal R, Kimbell J. Aerodynamic effects of inferior turbinate reduction: Computational fluid dynamics simulation. Arch Otolaryngol Head Neck. 2005 Dec-1;131(12):1102-7.

14. Simmen D, Scherrer JL, Moe K, Heinz B. A dynamic and direct visualization model for the study of nasal airflow. Arch Otolaryngol Head Neck. 1999 Sep-1;125(9):1015-21.

15. Kelly JT, Prasad AK, Wexler AS. Detailed flow patterns in the nasal cavity. J Appl Physiol. 2000 Jul-1;89(1):323-37.

16. Nunez D, Bradley PJ. A randomized clinical trial of turbinectomy for compensatory turbinate hypertrophy in patients with anterior septal deviations. Clin Otolaryngol. 2000 12 April 2000.

17. Munson, Young, Okiishi, editors. Fundamentals of fluid mechanics. ; 2006.

18. Fox RW, McDonald AT, Pritchard PJ, editors. Introduction to fluid mechanics. 6th ed. Hoboken, New Jersey: John Wiley and Sons Inc.; 2000.

19. Cowling R, Soria J. In: Flow visualization through model abdominal aortic anuerysm. 7-9 December 2005; ; 2005.

20. Oertel H, Spiegel K, Donisi S. Modeling the human cardiac fluid mechanic. ; 2006.

21. Heraty KB, Quinlan NJ. In: Experimental modelling of airflow in respiratory bifurcations. January 27-28, 2006; ; 2006.

22. PIV investigation of oscillating within a 3D lung multiple bifurcations model [homepage on the Internet]. . 2002. Available from: http://in3.dem.ist.utl.pt/lxlaser2002/papers/paper_19_1.pdf.

23. Adler K, Schroder W, Brucker C. In: DPIV measurements of dynamic flow patterns in a realistic model of the lung airways down to the 6th generation. June 26-29, 2006.

APPENDIX A: SCALING METHODS

To scale the volumetric flow rate using the Reynolds Number:

$$\mathrm{Re}_d = \frac{4 \times Q}{\pi \times d \times \nu}$$

$$\frac{4 \times Q_N}{\pi \times d_N \times \nu_{Air}} = \frac{4 \times Q_M}{\pi \times d_M \times \nu_W}$$

$$Q_M = \frac{4 \times Q_N}{\pi \times d_N \times \nu_{Air}} \times \frac{(\pi \times d_M \times \nu_W)}{4}$$

$$d_M = 2 \times d_N$$

$$Q_M = \frac{Q_N}{d_N \times \nu_{Air}} \times (2 \times d_N \times \nu_W)$$

$$Q_M = \frac{Q_N}{\nu_{Air}} \times (2 \times \nu_W)$$

$\nu_{Air} = 1.52 \times 10^{-5}$ m^2/s at 21.1°C (70 °F)

$\nu_W = 9.817 \times 10^{-7}$ m^2/s at 21.1 deg C (70 deg F)

$$Q_M = \frac{Q_N}{\nu_{Air}} \times (2 \times \nu_W)$$

To scale the frequency using the Womersley Number:

$$\alpha = R \times \sqrt{\frac{\omega}{\nu}}$$

$$R_N \times \sqrt{\frac{\omega_N}{\nu_{Air}}} = R_M \times \sqrt{\frac{\omega_M}{\nu_W}}$$

$$R_M = 2 \times R_N$$

$$R_N \times \sqrt{\frac{\omega_N}{\nu_{Air}}} = 2 \times R_N \times \sqrt{\frac{\omega_M}{\nu_W}}$$

$$\sqrt{\frac{\omega_N}{\nu_{Air}}} = 2 \times \sqrt{\frac{\omega_M}{\nu_W}}$$

$$\omega_M = \left(\sqrt{\frac{\omega_N}{\nu_{Air}}} \times \frac{1}{2} \right)^2 \times \nu_W$$

$\nu_{Air} = 1.52 \times 10^{-5}$ m^2/s at 21.1°C (70 °F)

$\nu_W = 9.817 \times 10^{-7}$ m^2/s at 21.1°C (70 °F)

$$\omega_M = \frac{\omega_N}{\nu_{Air}} \times \frac{1}{4} \times \nu_W$$

$$\omega_M = \omega_N \times .01615$$

To scale the pressure using Euler's Constant:

$$E_u = \frac{P}{\rho \times V_F}$$

$$\frac{P_A}{\rho_A \times V_A^{\,2}} = \frac{P_W}{\rho_W \times V_W^{\,2}}$$

$$V_F = \frac{Q}{A}$$

$$V_A = \frac{Q_N}{A_N}$$

$$V_W = \frac{Q_M}{A_M} = \frac{Q_N \times .12917}{4 \times A_N}$$

$$\frac{P_A}{\rho_A \times \left(\frac{Q_N}{A_N}\right)^2} = \frac{P_W}{\rho_W \times \left(\frac{Q_N \times .12917}{4 \times A_N}\right)^2}$$

$$\frac{P_A}{\rho_A} = \frac{P_W}{\rho_W \times \left(\frac{.12917}{4}\right)^2}$$

$$P_W = \frac{P_A}{\rho_A} \times (.001043 \times \rho_W)$$

ρ_A = 1.1934 kg/cu m

ρ_W = 997.97 kg/cu m

$$P_W = .8722 \times P_A$$

APPENDIX B: FLOWRATE TO MOTOR SPEED CONVERSION

Through laboratory experiments, we tested to find the volume pumped per single rotation of the pump rotor. The raw data from these tests are shown below in Table 4.

Table 4: Pump Volume Test Data

Trial #	# of Rotations	Volume Pumped (mL)	Volume/Rotation (l)
1	10	14.5	.00145
2	10	14.5	.00145
3	10	14.5	.00145
4	15	21.5	.00143

Equation 11: Breathing Curve Motor Conversion

$$\omega = Q \times \frac{C}{V}$$

Where,

V = volume per cycle = .00145 L/rotation
ω = motor velocity (counts /sec)
C = counts per cycle = 4000 counts/rotation
Q =volume flowrate (L/sec)

From this, we were able to find the data points shown in Figure , which were then used to program the motor.

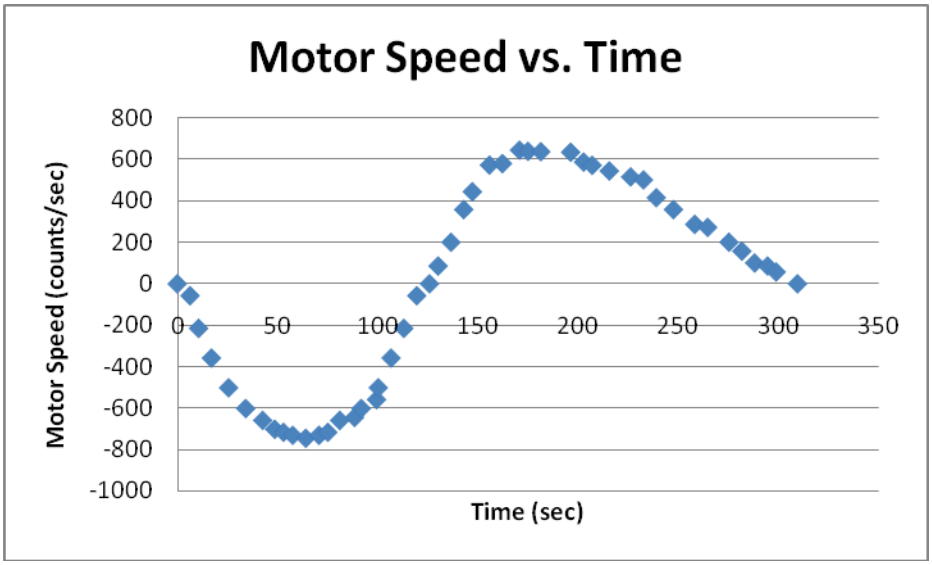

Figure 23: Motor Speed vs. Time